

Convolutionally Coded Multicarrier DS-CDMA Systems in a Multipath Fading Channel— Part I: Performance Analysis

Douglas N. Rowitch, *Member, IEEE*, and Laurence B. Milstein, *Fellow, IEEE*

Abstract—This paper presents a multicarrier asynchronous direct-sequence code-division multiple-access (DS-CDMA) system wherein the output of a convolutional encoder modulates multiple band-limited DS-CDMA waveforms, which are transmitted in parallel at different carrier frequencies. The receiver detects and combines signals for the desired user and feeds a soft-decision Viterbi decoder. The performance of this system is compared to that of a conventional single-carrier DS-CDMA system with a RAKE receiver, assuming a slowly varying frequency-selective Rayleigh fading channel and assuming the presence of additive white Gaussian noise and multiple-access interference. Results will demonstrate similar performance at roughly equal receiver complexity. Part II of this paper extends the comparison to include various forms of narrow-band interference.

Index Terms—CDMA, multicarrier, multipath fading.

I. INTRODUCTION

DIRECT-SEQUENCE code-division multiple access (DS-CDMA) has become a popular multiple-access signaling methodology due, in part, to its robustness against fading, anti-interference capability [1], and multiple-access capacity [2]. The large spreading bandwidths employed typically exceed the coherence bandwidth of the channel, so that the fading tends to be frequency selective. In such a situation, a RAKE receiver can be used to exploit path diversity and effectively combat the performance degradation due to multipath [1]. The anti-interference capability in a direct-sequence (DS) system is achieved by correlating the received signal with the predetermined spreading sequence, thus allowing the inherent processing gain of the system to attenuate the interference [2].

In this paper, we propose an alternative to the classical RAKE receiver, in that the available bandwidth is decomposed into a set of disjoint equi-width frequency sub-bands of

bandwidth approximately equal to the coherence bandwidth of the channel. Each sub-band of the channel is assumed to fade nonselectively and independently [3]. In short, path diversity is exchanged for frequency diversity, wherein forward error correction may be employed [4], [5].

This paper builds upon the previous work of Kondo and Milstein [3], in which they examined a multicarrier DS-CDMA system that applied repetition coding to transmit M band-limited DS-CDMA waveforms whose bandwidths summed to that of a comparable single-carrier DS-CDMA system. The receiver then maximal-ratio combined the test statistics of the M subcarrier receivers. This system was compared to a classical single-carrier DS-CDMA system employing a RAKE receiver, where the number of tones M was taken to be equal to the number of resolvable paths L in the single-carrier system. Performance was shown to be equivalent in the presence of additive white Gaussian noise (AWGN) and multiple-access interference (MAI). However, the multicarrier system exhibited superior performance in the presence of partial-band interference, since the maximal-ratio combiner will naturally attenuate outputs of the subset of tones experiencing the interference. Thus, at roughly equivalent receiver complexity, the multicarrier system was shown to effectively combat the partial-band interference without the added complexity of a front-end interference suppression or notch filter.

In [4] and [5], the authors introduced an extension of the work by Kondo and Milstein in which the symbols transmitted over the M multicarrier tones were modulated by a rate $1/M$ convolutional encoder instead of a repetition code. This system was shown to effectively combat multiple-access and partial-band interference but was more sensitive to the effects of Rayleigh fading when compared to a similarly coded single-carrier system. This was because the energy transmitted for a code symbol in the single-carrier system was distributed among several independently fading paths, whereas a code symbol for the coded multicarrier system was received via a single flat fading path.

In this paper, we propose a hybrid of the above-mentioned multicarrier schemes in which each convolutionally encoded symbol is also repetition-coded and transmitted over independent frequency diversity branches.

The current literature on multicarrier modulation (MCM) as applied to DS-CDMA may be classified into two general areas, depending upon whether time-domain or frequency-domain spreading is employed. These classes of DS-CDMA systems

Paper approved by B. D. Woerner, the Editor for Wireless Spread Spectrum of the IEEE Communications Society. Manuscript received October 17, 1996; revised July 6, 1998. This work was supported in part by the National Science Foundation under Grant NCR-923140 and in part by the Focused Research Initiative on Wireless Multimedia Networks under Grant DAAH04-95-1-0248. This paper was presented in part at the 1995 International Symposium on Information Theory, Whistler, BC, Canada, September 1995, and at MILCOM'96, McLean, VA, November 1996.

D. N. Rowitch was with the Department of Electrical and Computer Engineering, University of California at San Diego, La Jolla, CA 92093-0407 USA. He is now with Qualcomm Inc., San Diego, CA 92121 USA (e-mail: drowitch@qualcomm.com).

L. B. Milstein is with the Department of Electrical and Computer Engineering, University of California at San Diego, La Jolla, CA 92093-0407 USA (e-mail: milstein@ece.ucsd.edu).

Publisher Item Identifier S 0090-6778(99)07800-9.

are discussed and surveyed in [3] and [6]. Both classes of MCM systems show a similar capability to mitigate the effects of fading; however, the time-spreading class will, in general, employ a smaller number of carriers relative to the frequency spreading class and thus be lower in complexity. The system proposed in this paper belongs to the time-spreading class of systems.

As in [3], we do not require that the subcarrier frequencies satisfy an orthogonality condition, since orthogonality will typically be corrupted due to multipath propagation, Doppler shifts, and phase jitter [7]. Instead, we employ band-limited pulse shaping and assign subcarrier frequencies such that the respective sub-bands do not overlap. In this manner, adjacent channel interference is suppressed, obviating the need for an orthogonality assumption.

An overview of the organization of this paper is as follows. Section II introduces the system model for the proposed multicarrier DS-CDMA system, and Section III presents a performance analysis of the system. In Section IV, we compare the coded multicarrier system with a similarly coded single-carrier system employing a RAKE receiver. Section V presents numerical results for the selection of multicarrier system parameters and for the comparison to a conventional single-carrier system. Finally, in Section VI, we present the conclusions.

II. SYSTEM MODEL

A. System Overview

In the literature, one finds wide-band CDMA systems proposed either to realize an overlay system [8], [3], [10] in which DS-CDMA waveforms are overlaid onto existing narrow-band signals to enhance the net capacity, or to combat multipath [9]. A multicarrier system can be considered as one realization of such a wide-band DS system. Fig. 1(a) depicts a band-limited DS waveform of a wide-band single-carrier system in the frequency-domain, where the bandwidth W_{SC} is given by

$$W_{SC} = (1 + \beta) \frac{1}{T_c}. \quad (1)$$

In (1), β is the rolloff factor of the chip wave-shaping filter ($0 < \beta \leq 1$), and T_c is the chip duration of the single-carrier system.

In the multicarrier system proposed, we divide W_{SC} into MR equi-width disjoint frequency sub-bands, as shown in Fig. 1(b). Note that while the multicarrier system is depicted as using a contiguous spectrum, this need not be the case, in general. The ability to make use of a noncontiguous spectrum to achieve a given total bandwidth represents an advantage over the single-carrier approach (which requires a contiguous spectrum). The bandwidth of each frequency sub-band W_{MC} is given by

$$W_{MC} = \frac{W_{SC}}{MR} = (1 + \beta) \frac{1}{MRT_c}. \quad (2)$$

Note that MRT_c is the chip duration of the multicarrier system, and MR is the total number of subcarriers. The

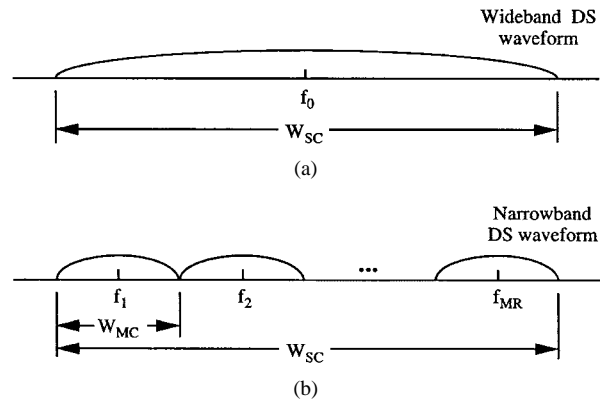


Fig. 1. Power spectral density of (a) single-carrier DS waveform and (b) multicarrier DS waveform.

parameter M will specify the number of convolutionally coded symbols per input data symbol, and $2R$ will specify the number of frequency diversity branches per coded symbol, as will be seen in the following section.

B. Transmitter

Across each of the MR carrier frequencies, we transmit an in-phase and quadrature DS-CDMA signal, such that two *distinct* binary symbols may be transmitted at a given carrier frequency. The transmitter for the k th user is shown in Fig. 2(a). The binary data sequence $d_m^{(k)}$ (where $m \equiv \lfloor n/N \rfloor$) is input to a rate $1/M$ convolutional encoder. The output code symbols are interleaved and serial-to-parallel converted such that M parallel code symbols $\{b_{i,m}^{(k)}\}_{i=1}^M$ may be transmitted simultaneously. Each of the M code symbols, in turn, is replicated via a rate $1/(2R)$ repetition code. The $2MR$ code symbols are then mapped to in-phase and quadrature DS-CDMA modulators such that each of the M convolutionally coded symbols is transmitted over $2R$ independent frequency diversity branches. The code symbols are mapped to subcarriers so as to maximize the separation in frequency between repetition code symbols for each respective convolutional code symbol. One such mapping is illustrated in Fig. 2(c) for the case $M = 6$ and $R = 2$, where the numbers identify the mapping of convolutional code symbols to in-phase and quadrature subcarriers. The symbol mapper will be treated in detail later in this section. Note that each user simultaneously uses all MR subcarriers and thus occupies the entire wide-band spectrum.

The in-phase and quadrature (I & Q) modulator for the ν th subcarrier ($1 \leq \nu \leq MR$) of the k th user, shown in Fig. 2(b), receives two *distinct* binary code symbols (± 1), which are multiplied by a pseudorandom spreading sequence $c_n^{(k)}$ such that there are N chips per code symbol, and each user has a unique spreading sequence. The resulting sequence $(a_{\nu, \lfloor n/N \rfloor} - j\tilde{a}_{\nu, \lfloor n/N \rfloor}) \cdot c_n^{(k)}$ modulates an impulse train, where the energy per chip is E_c and the period of the impulse train is MRT_c . After passing through a chip wave-shaping filter $H(f)$, the baseband DS-CDMA waveform is upconverted to subcarrier frequency f_ν and multiplexed with the other subcarrier signals. Note that efficient schemes exist for the

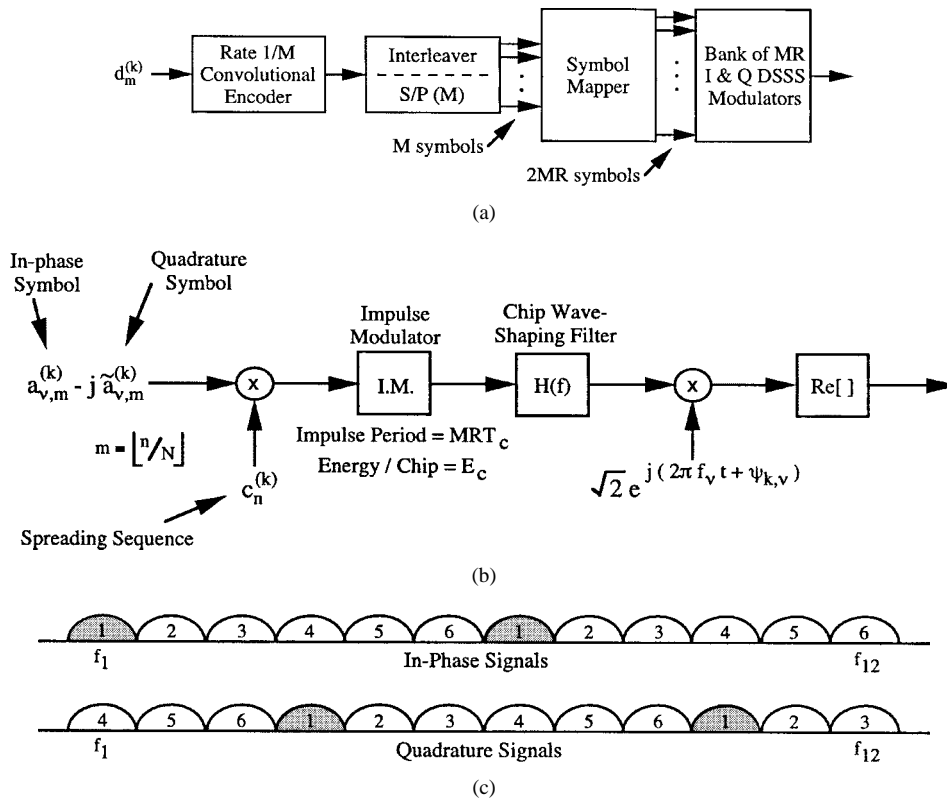


Fig. 2. Transmitter block diagram. (a) Transmitter for the k th user. (b) I & Q DSSS modulator at subcarrier f_v ($1 \leq v \leq MR$). (c) Example code symbol to subcarrier mapping.

synthesis of multicarrier waveforms which make use of the discrete Fourier transform (DFT) [11]; the transmitter and receiver structure used in this paper, while not an efficient implementation, serve to simplify the system performance analysis.

We now treat the symbol mapper in greater detail. Let $\{f_\nu\}_{\nu=1}^{MR}$ be an ordered set of carrier frequencies such that $f_\nu < f_{\nu+1}$. We specify the mapping of the M convolutional code symbols $b_{i,m}^{(k)}$, $1 \leq i \leq M$ into the MR in-phase ($a_{\nu,m}^{(k)}$) and quadrature ($\tilde{a}_{\nu,m}^{(k)}$) output symbols, $1 \leq \nu \leq MR$, as follows:

$$\begin{aligned} a_{\nu,m}^{(k)} &= b_{f(\nu),m}^{(k)} \\ \tilde{a}_{\nu,m}^{(k)} &= b_{\tilde{f}(\nu),m}^{(k)} \end{aligned} \quad (3)$$

where

$$\begin{aligned} f(\nu) &= 1 + \{\nu - 1, \text{mod } M\} \\ \tilde{f}(\nu) &= 1 + \{\nu - 1 + \lfloor M/2 \rfloor, \text{mod } M\}. \end{aligned} \quad (4)$$

This is illustrated in the following example for the case $M = 6$ and $R = 2$, where dropping the m and (k) indices for simplicity, we obtain the mapping

$$\begin{aligned} \mathbf{a} &= \{b_1, b_2, b_3, b_4, b_5, b_6, b_1, b_2, b_3, b_4, b_5, b_6\} \\ \tilde{\mathbf{a}} &= \{b_4, b_5, b_6, b_1, b_2, b_3, b_4, b_5, b_6, b_1, b_2, b_3\}. \end{aligned} \quad (5)$$

It can thus be seen, for example, that the first of the six convolutionally coded symbols is transmitted over subcarrier frequencies f_1, f_4, f_7 , and f_{10} . This represents one of many

possible mappings which maximize the separation in frequency of the transmitted diversity branches for a given outer code symbol and, thus, maximizes the diversity effect for each outer code symbol. The need for the interleaver in Fig. 2(a) is apparent when one notes, for example, that the first and fourth outer code symbols are transmitted over the same four carriers, and thus, the fading effects on that symbol pair will be identical even though the four individual fading envelopes are assumed to be uncorrelated. The interleaver will serve to distribute outer code symbols in time such that the effects of deep fades are distributed among code words separated in time. It is seen that a factor two increase in diversity order is picked up by using the in-phase and quadrature architecture over the binary phase-shift keying architecture proposed in [4] and [5].

C. Channel

The channel is assumed to be a slowly varying frequency-selective Rayleigh fading channel, with respect to the single-carrier system, with delay spread of T_m as in [3]. We assume that the single-carrier system experiences L th-order path diversity, where [12]

$$L = \lceil T_m/T_c \rceil \quad (6)$$

and $\lceil \eta \rceil$ represents the smallest integer greater than or equal to η . Then, the complex low-pass equivalent impulse response of the channel can be modeled as [1]

$$c(t) = \sum_{\ell=0}^{L-1} \zeta_\ell \delta(t - \ell T_c) \quad (7)$$

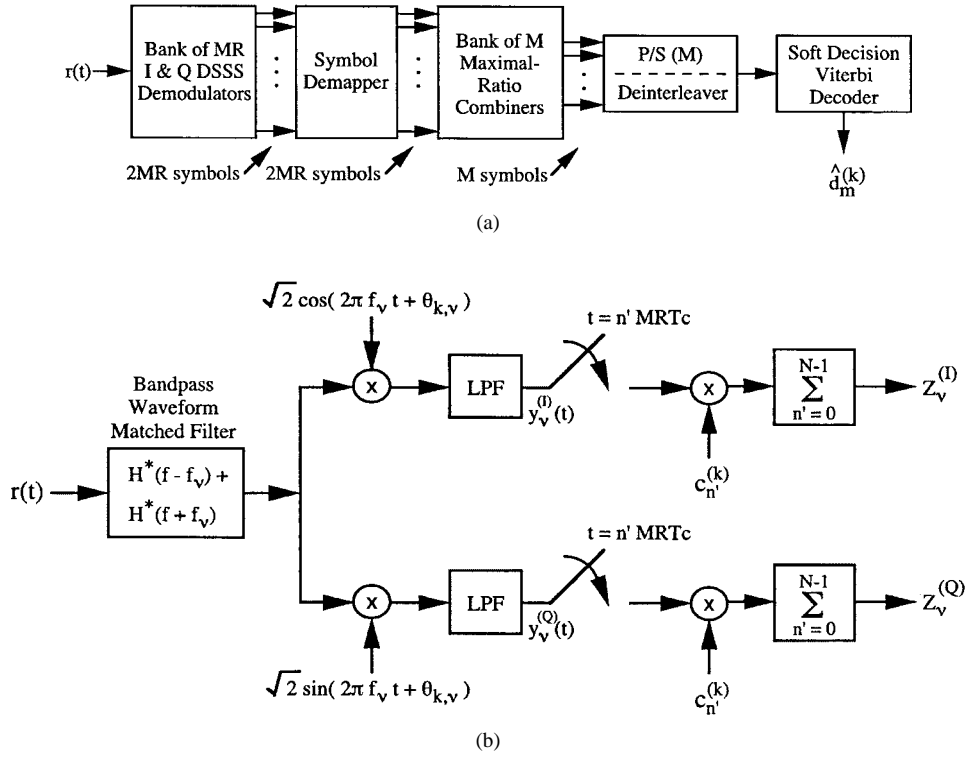


Fig. 3. Receiver block diagram. (a) Receiver for the k th user. (b) I & Q DSSS demodulator at subcarrier f_v ($1 \leq v \leq MR$).

where the $\{\zeta_\ell\}$ are zero-mean complex Gaussian random variables.

On the other hand, a frequency-domain channel model can be characterized by the coherence bandwidth $(\Delta f)_c$, which is given by [12]

$$(\Delta f)_c \approx \frac{1}{T_m}. \quad (8)$$

As in [3], we constrain M and R to satisfy the following conditions:

- Each sub-band of a multicarrier system has no selectivity, i.e., $T_m/(MRT_c) \leq 1$.
- All sub-bands are subject to independent fading, i.e., $W_{MC} \geq (\Delta f)_c$.

From (2) and (8), these two conditions are satisfied if

$$\frac{T_m}{T_c} \leq MR \leq (1 + \beta) \frac{T_m}{T_c}. \quad (9)$$

Noting from (6) that $T_m/T_c \leq L \leq T_m/T_c + 1$, we ensure the left inequality of (9) by choosing $MR = L$. To ensure the right inequality, we choose β to be large enough such that $\beta \geq T_c/T_m$, which implies $T_m/T_c + 1 \leq (1 + \beta)T_m/T_c$.

Under the above assumptions, the transfer function of the ν th frequency band for the k th user is given by $\zeta_{k,\nu} \equiv \alpha_{k,\nu} e^{j\beta_{k,\nu}}$, where $\alpha_{k,\nu}$ and $\beta_{k,\nu}$ are, respectively, an independently, identically distributed (i.i.d.) Rayleigh random variable with unit second moment and an i.i.d. uniform random variable over $[0, 2\pi)$.

The received signal is then given by

$$r(t) = \sum_{k=1}^{K_u} \left\{ \sqrt{2E_c} \sum_{n=-\infty}^{\infty} c_n^{(k)} h(t - nMRT_c - \tau_k) \cdot \sum_{\nu=1}^{MR} \alpha_{k,\nu} \left[a_{\nu, [n/N]}^{(k)} \cos(2\pi f_\nu t + \theta_{k,\nu}) + \tilde{a}_{\nu, [n/N]}^{(k)} \sin(2\pi f_\nu t + \theta_{k,\nu}) \right] \right\} + n_W(t) \quad (10)$$

where $h(t)$ is the impulse response of the chip wave-shaping filter, the $\{\tau_k\}$ are asynchronous delays assumed to be i.i.d. uniform random variables over $[0, MRT_c)$, $\theta_{k,\nu} = \psi_{k,\nu} + \beta_{k,\nu}$, and $n_W(t)$ is AWGN with two-sided power spectral density of $\eta_0/2$.

D. Receiver

The receiver of the k th user is shown in Fig. 3(a). There is an in-phase and quadrature correlator for each of the MR carrier frequencies. Each I & Q correlator [see Fig. 3(b)] consists of a bandpass matched filter operation, followed by coherent demodulation,¹ sampling, despreading, and summing. The $2MR$ receiver test statistics are then demapped into M partitions of $2R$ terms in accordance with the mapping rule of (3). Each partition is input to a maximal-ratio combiner producing a diversity combined test statistic corresponding to each of the M convolutional code symbols. The resulting M

¹For systems of practical interest, low-power unmodulated pilot DS-CDMA signals may be multiplexed with the data signals at each subcarrier to make coherent demodulation viable.

diversity combined outputs are deinterleaved and ultimately feed metric calculations in the soft-decision Viterbi decoder.

We assume that the chip wave-shaping filter $H(f)$ satisfies the Nyquist criterion and is of unit energy. We further define

$$x(t) \Leftrightarrow X(f) \equiv |H(f)|^2 \quad (11)$$

and assume that $X(f)$ is bandlimited to W' , where $W' \leq W_{MC}/2$. This implies that the DS waveforms do not overlap in frequency, and thus, adjacent channel interference may be ignored. Since $X(f)$ satisfies the Nyquist criterion, we may ignore interchip interference as well.

III. ANALYSIS

A. Output of the Chip Matched Filter

We evaluate the performance of the first user ($k = 1$), assuming perfect carrier, code, and bit synchronization. Then the output, prior to sampling, from the in-phase and quadrature correlator branches at the ν th subcarrier frequency, $y_\nu^{(I)}(t)$ and $y_\nu^{(Q)}(t)$, are given by

$$y_\nu^{(I)}(t) = S_{y_\nu}^{(I)}(t) + I_{y_\nu}^{(I)}(t) + N_{y_\nu}^{(I)}(t) \quad (12)$$

and

$$y_\nu^{(Q)}(t) = S_{y_\nu}^{(Q)}(t) + I_{y_\nu}^{(Q)}(t) + N_{y_\nu}^{(Q)}(t) \quad (13)$$

respectively, where

$$S_{y_\nu}^{(I)}(t) = \sqrt{E_c} \alpha_{1,\nu} \sum_{n=-\infty}^{\infty} a_{\nu, \lfloor n/N \rfloor}^{(1)} c_n^{(1)} x(t - nMRT_c) \quad (14)$$

$$S_{y_\nu}^{(Q)}(t) = \sqrt{E_c} \alpha_{1,\nu} \sum_{n=-\infty}^{\infty} \tilde{a}_{\nu, \lfloor n/N \rfloor}^{(1)} c_n^{(1)} x(t - nMRT_c) \quad (15)$$

$$N_{y_\nu}^{(I)}(t) = Lp\left\{n_{W_\nu}(t)\sqrt{2}\cos(2\pi f_\nu t + \theta_{1,\nu})\right\} \quad (16)$$

and

$$N_{y_\nu}^{(Q)}(t) = Lp\left\{n_{W_\nu}(t)\sqrt{2}\sin(2\pi f_\nu t + \theta_{1,\nu})\right\} \quad (17)$$

represent in-phase and quadrature components due to the desired signal (S) and additive white Gaussian noise (N), respectively. In the above equations, we have assumed, without loss of generality, that $\tau_1 = 0$. The term $n_{W_\nu}(t)$ represents the band-limited process obtained by convolving the additive white Gaussian noise $n_W(t)$ with the impulse response of the ν th bandpass chip filter. Finally, $Lp\{\cdot\}$ denotes a low-pass filter operation to remove double-frequency terms.

The in-phase MAI (I) in (12) will contain components due to *both* in-phase and quadrature signals of the $K_u - 1$ interfering users, since those signals will, in general, be out-of-phase with that of the user-of-interest. The in-phase interference component $I_{y_\nu}^{(I)}(t)$ is given by

$$I_{y_\nu}^{(I)}(t) = \sum_{k=2}^{K_u} \left\{ \sqrt{E_c} \sum_{n=-\infty}^{\infty} c_n^{(k)} \alpha_{k,\nu} x(t - nMRT_c - \tau_k) \cdot \left[a_{\nu, \lfloor n/N \rfloor}^{(k)} \cos(\phi_{k,\nu}) + \tilde{a}_{\nu, \lfloor n/N \rfloor}^{(k)} \sin(\phi_{k,\nu}) \right] \right\} \quad (18)$$

where $\phi_{k,\nu} = \theta_{k,\nu} - \theta_{1,\nu}$. To characterize the interference, we assume the spreading sequences of the multiple-access interferers to be statistically independent, random binary sequences, whereupon the product of those sequences with the code symbols are random binary sequences. We may thus drop the code symbols from (18) and define $\xi_{k,\nu}^{(I)} \triangleq \alpha_{k,\nu} \cos(\phi_{k,\nu}) \pm \alpha_{k,\nu} \sin(\phi_{k,\nu})$, $2 \leq k \leq K_u$. It can be shown, based on the statistics of the $\{\alpha_{k,\nu}\}$ and $\{\phi_{k,\nu}\}$, that the $\{\xi_{k,\nu}^{(I)}\}$ are i.i.d. zero-mean Gaussian random variables with variance equal to unity. Equation (18), therefore, is essentially equivalent to

$$I_{y_\nu}^{(I)}(t) = \sum_{k=2}^{K_u} \left\{ \sqrt{E_c} \xi_{k,\nu}^{(I)} \sum_{n=-\infty}^{\infty} c_n^{(k)} x(t - nMRT_c - \tau_k) \right\}. \quad (19)$$

It is easily shown that the MAI in the quadrature channel may be similarly characterized as

$$I_{y_\nu}^{(Q)}(t) = \sum_{k=2}^{K_u} \left\{ \sqrt{E_c} \xi_{k,\nu}^{(Q)} \sum_{n=-\infty}^{\infty} c_n^{(k)} x(t - nMRT_c - \tau_k) \right\} \quad (20)$$

where $\xi_{k,\nu}^{(Q)} \triangleq \alpha_{k,\nu} \sin(\phi_{k,\nu}) \mp \alpha_{k,\nu} \cos(\phi_{k,\nu})$.

B. Signal Out of the ν th Correlator and Its Statistics

In this subsection, we evaluate the statistics of the signal out of the ν th in-phase and quadrature correlators, $Z_\nu^{(I)}$ and $Z_\nu^{(Q)}$, respectively, which can be written as

$$Z_\nu^{(I)} = S_{Z_\nu}^{(I)} + I_{Z_\nu}^{(I)} + N_{Z_\nu}^{(I)} \quad (21)$$

and

$$Z_\nu^{(Q)} = S_{Z_\nu}^{(Q)} + I_{Z_\nu}^{(Q)} + N_{Z_\nu}^{(Q)} \quad (22)$$

where

$$\begin{aligned} S_{Z_\nu}^{(I)} &= \sum_{n'=0}^{N-1} c_{n'}^{(1)} S_{y_\nu}^{(I)}(n'MRT_c) \\ S_{Z_\nu}^{(Q)} &= \sum_{n'=0}^{N-1} c_{n'}^{(1)} S_{y_\nu}^{(Q)}(n'MRT_c) \\ I_{Z_\nu}^{(I)} &= \sum_{n'=0}^{N-1} c_{n'}^{(1)} I_{y_\nu}^{(I)}(n'MRT_c) \\ I_{Z_\nu}^{(Q)} &= \sum_{n'=0}^{N-1} c_{n'}^{(1)} I_{y_\nu}^{(Q)}(n'MRT_c) \\ N_{Z_\nu}^{(I)} &= \sum_{n'=0}^{N-1} c_{n'}^{(1)} N_{y_\nu}^{(I)}(n'MRT_c) \\ N_{Z_\nu}^{(Q)} &= \sum_{n'=0}^{N-1} c_{n'}^{(1)} N_{y_\nu}^{(Q)}(n'MRT_c). \end{aligned} \quad (23)$$

Note that while we assume the $\{c_n^{(k)}, k = 2, \dots, K_u\}$ to be independent random binary sequences, we take the spreading sequence for the desired user $c_n^{(1)}$ to be deterministic.

It can be shown that the conditional mean of $Z_\nu^{(I)}$, conditioned on $\alpha_{1,\nu}$ and the code symbol $a_{\nu, \lfloor n/N \rfloor}^{(1)}$, is given by [6]

$$E\left[Z_\nu^{(I)} \mid \alpha_{1,\nu}, a_{\nu, \lfloor n/N \rfloor}^{(1)}\right] = \pm N \sqrt{E_c} \alpha_{1,\nu} \quad (24)$$

where the algebraic sign is determined by the code symbol $a_{\nu, \lfloor n/N \rfloor}$, which is constant over the N chips. A similar result holds for the quadrature channel output.

The remaining outputs, due to MAI ($I_{Z_\nu}^{(I)}$) and AWGN ($N_{Z_\nu}^{(I)}$), are assumed to be mutually, statistically independent random variables. The latter term is a Gaussian random variable by definition, since it represents the response of a linear time-invariant system to an input zero-mean Gaussian random process. The MAI is asymptotically Gaussian in the number of users K_u , as shown in [6]. It is further shown in [6] that the set of random variables $\{I_{Z_\nu}^{(I)}, I_{Z_\nu}^{(Q)}\}$, across all subcarriers, is asymptotically, *jointly* Gaussian in K_u . Therefore, conditioned on the amplitude of the fading envelope and the transmitted code symbol, $Z_\nu^{(I)}$ is approximately Gaussian, where the approximation is valid for a large number of users K_u and is perfect for $K_u = 1$. Hence, we must determine the conditional variance of $Z_\nu^{(I)}$ to completely specify the statistics of the in-phase correlator output. The conditional variance of $Z_\nu^{(I)}$, conditioned upon $\alpha_{1,\nu}$, is given by

$$\begin{aligned} \text{var}\{Z_\nu^{(I)} \mid \alpha_{1,\nu}\} &\equiv (\sigma_\nu^{(I)})^2 \\ &= \text{var}\{I_{Z_\nu}^{(I)} + N_{Z_\nu}^{(I)} \mid \alpha_{1,\nu}\} \\ &= \text{var}\{I_{Z_\nu}^{(I)} \mid \alpha_{1,\nu}\} + \text{var}\{N_{Z_\nu}^{(I)} \mid \alpha_{1,\nu}\}. \end{aligned} \quad (25)$$

The conditional variance for the MAI component is [6]

$$\begin{aligned} \text{var}\{I_{Z_\nu}^{(I)} \mid \alpha_{1,\nu}\} \\ = NR_{I_{y_\nu}}(0) + 2 \sum_{\ell=1}^{N-1} R_{I_{y_\nu}}(\ell MRT_c) \sum_{n'=\ell}^{N-1} c_{n'}^{(1)} c_{n'-\ell}^{(1)} \end{aligned} \quad (26)$$

where $R_{I_{y_\nu}}(\tau)$ is the autocorrelation function of $I_{y_\nu}^{(I)}(t)$ and is defined as the inverse Fourier transform of the power spectral density of $I_{y_\nu}^{(I)}(t)$

$$S_{I_{y_\nu}}(f) = \frac{(K_u - 1)E_c}{MRT_c} |X(f)|^2. \quad (27)$$

Equation (27) is derived in [6], as is $R_{I_{y_\nu}}(\tau)$ (in closed form) for an explicit class of wave-shaping filters considered in this paper.

Lastly, the conditional variance for the AWGN component is

$$\text{var}\{N_{Z_\nu}^{(I)} \mid \alpha_{1,\nu}\} = \frac{N\eta_0}{2} \quad (28)$$

where $R_{N_{y_\nu}}(\tau) = \eta_0/2 \cdot x(\tau)$ is the autocorrelation function of $N_{y_\nu}^{(I)}(t)$.

Since neither of the variance expressions depend on the fade amplitude $\alpha_{1,\nu}$, the variance in (25) is unconditional. Furthermore, it can be shown that the variance is identical

in both in-phase and quadrature channels; that is, $(\sigma_\nu^{(Q)})^2 = (\sigma_\nu^{(I)})^2 \triangleq \sigma_\nu^2$.

We now wish to consider the joint statistics of the inputs to a given maximal-ratio combiner. To do this, we must define the mechanism by which the symbol demapper partitions the $2MR$ correlator outputs $\{Z_\nu^{(I)}, Z_\nu^{(Q)}\}_{\nu=1}^{MR}$ into M partitions of $2R$ terms. Let $Z_{i,j}$ denote the correlator output corresponding to the j th repetition of the i th convolutional code symbol, where $1 \leq i \leq M$ and $1 \leq j \leq 2R$. Then, consequent on the mapping defined in (3), we have for each i

$$Z_{i,j} = \begin{cases} Z_{\nu(i,j)}^{(I)}, & \text{for } j = 1, \dots, R \\ Z_{\nu(i,j)}^{(Q)}, & \text{for } j = R+1, \dots, 2R \end{cases} \quad (29)$$

where the function $\nu(i, j)$ maps the indices i and j into the appropriate frequency sub-band index $1 \leq \nu \leq MR$ and is given by

$$\begin{aligned} \nu(i, j) = \\ \begin{cases} i + (j-1)M, & j \leq R \\ i + (j-R)M - \lfloor M/2 \rfloor, & j > R, \quad i \leq \lfloor M/2 \rfloor \\ i + (j-R-1)M - \lfloor M/2 \rfloor, & j > R, \quad i > \lfloor M/2 \rfloor \end{cases} \end{aligned} \quad (30)$$

Consider any pair of random variables, Z_{i,j_1} and Z_{i,j_2} , where $j_1 \neq j_2$, while holding i fixed. Any such pair of random variables corresponds to receiver outputs from disjoint frequency sub-bands; this implies independence of the AWGN components. Moreover, the carrier frequencies associated with each pair of random variables are separated by at least the coherence bandwidth of the channel, as guaranteed by inequality (9); this implies that the MAI components are uncorrelated (note that the assumption of independent transmission carrier phases for every subcarrier of every user is sufficient to guarantee this last result, even in the absence of Rayleigh fading). From this, we conclude that the pair of random variables Z_{i,j_1} and Z_{i,j_2} are uncorrelated and, thus, asymptotically independent [6]. Therefore, the $2R$ correlator outputs which are input to the i th maximal-ratio combiner are conditionally, asymptotically, independent, jointly Gaussian random variables.

C. Inner Repetition Code Test Statistics

Define the test statistic for the maximal-ratio combiner corresponding to the i th convolutionally coded symbol as

$$Z_i = \sum_{j=1}^{2R} g_{i,j} Z_{i,j} \quad (31)$$

where the optimal gain coefficients $g_{i,j}$ are selected according to

$$g_{i,j} = \frac{E\{Z_{i,j} \mid \alpha_{1,\nu(i,j)}\}}{\text{var}\{Z_{i,j} \mid \alpha_{1,\nu(i,j)}\}} \quad (32)$$

as shown in [3]. We assume perfect channel state information, such that the estimates of the gain coefficients (omitting constant multipliers) are simply

$$g_{i,j} = \frac{\alpha_{1,\nu(i,j)}}{\sigma_{\nu(i,j)}^2}. \quad (33)$$

In the absence of additive narrow-band interference (NBI), the variance estimate in the denominator of (33) may be omitted. However, for theoretical analysis, we assume that the variances across different subcarriers are, in general, unequal, such that theoretical results can be obtained both in the absence (Part I) and presence (Part II) of NBI. Therefore, Z_i , as defined in (31), is a weighted sum of uncorrelated (and thus independent) conditionally, jointly Gaussian random variables and has the distribution

$$Z_i \mid \gamma_i \xrightarrow{K_u \rightarrow \infty} N(\pm N\sqrt{E_c}\gamma_i, \gamma_i) \quad (34)$$

where the \pm sign is a function of the i th convolutional code symbol, and

$$\gamma_i \triangleq \sum_{j=1}^{2R} \frac{\alpha_{1,\nu(i,j)}^2}{\sigma_{\nu(i,j)}^2}. \quad (35)$$

D. Soft-Decision Viterbi Decoder Metrics

With sufficient interleaving of coded symbols output from the convolutional encoder, we assume that the vector of M deinterleaved maximal-ratio combined receiver outputs, at time index ℓ , \bar{Z}_ℓ , represent uncorrelated (and therefore independent), conditionally, jointly Gaussian random variables with distribution given by (34).

Then, the branch metric for the r th path through the decoder trellis at time index ℓ is given by

$$\mu_\ell^{(r)} = \log P(\bar{Z}_\ell \mid \bar{B}_\ell^{(r)}) \quad (36)$$

where $\bar{B}_\ell^{(r)}$ represents the vector of M convolutionally coded symbols at time index ℓ corresponding to the r th path. We evaluate (36) in terms of the joint conditional distribution of \bar{Z}_ℓ , conditioned on $\bar{B}_\ell^{(r)}$ and the $\{\gamma_{i,\ell}\}$, as follows:

$$\mu_\ell^{(r)} = \sum_{i=1}^M \log \left\{ \frac{1}{\sqrt{2\pi\gamma_{i,\ell}}} e^{-(1/(2\gamma_{i,\ell})) (Z_{i,\ell} - b_{i,\ell}^{(r)} N\sqrt{E_c}\gamma_{i,\ell})^2} \right\} \quad (37)$$

where the subscript ℓ is introduced to denote a time index, and $b_{i,\ell}^{(r)}$ represents the i th coded symbol of the r th trellis path at time index ℓ for the first (i.e., desired) user. Expanding (37), discarding components which are not dependent on the path index r (since those terms will be common to all branch metrics), as well as constant multiplicative factors, we obtain

$$\mu_\ell^{(r)} = \sum_{i=1}^M (Z_{i,\ell} \cdot b_{i,\ell}^{(r)}) \quad (38)$$

which is the well-known inner-product branch metric for the AWGN channel [12].

Next, we define the r th path metric as

$$U^{(r)} = \sum_{\ell=1}^B \mu_\ell^{(r)} \quad (39)$$

where B can be interpreted either as a tailed-off block size or as a truncated depth in the trellis in which all likely error paths remerge with the all-zeros state.

E. Coded Performance

Since linear, binary convolutional codes can be shown to satisfy the criteria of a group code [13], we may evaluate coded performance by assuming that the all-zeros sequence ($r = 0$) is transmitted and consider the event that the decoder selects some competing path ($r = 1$).

The probability of selecting a given competing path over the all-zeros path is given by

$$P(U^{(1)} - U^{(0)} \geq 0) = P\left(\sum_{\ell=1}^B \sum_{i=1}^M Z_{i,\ell} [b_{i,\ell}^{(1)} - b_{i,\ell}^{(0)}] \geq 0\right). \quad (40)$$

Note that the expression in square brackets vanishes except at the locations corresponding to code symbol errors in the competing path. If we discard the vanishing terms and partition the remaining terms by code symbol, such that there are d_i code symbol errors in the set of $\{Z_{i,\ell}\}$, $1 \leq \ell \leq B$, for each i in the range $1 \leq i \leq M$, then the above probability can be expressed as

$$P(U^{(1)} - U^{(0)} \geq 0) = P\left(\sum_{i=1}^M \sum_{\ell=1}^{d_i} Z_{i,\hat{\ell}} \leq 0\right) \quad (41)$$

where the index $\hat{\ell}$ maps to the appropriate location corresponding to the d_i code symbol errors, for each i . The reason for partitioning by code symbol is that the average signal-to-noise ratio (SNR) associated with each code symbol may be different due to the presence of NBI (see Part II of this paper).

To upper bound the performance of the proposed system, we apply the Chernoff bound on the above probability for a specific set of distances d_1, d_2, \dots, d_M . This bound is then used in conjunction with a code transfer function to union bound the first error event probability and probability of bit error [12], [13].

We, therefore, define the probability in (41), for an explicit distance profile, as follows:

$$P(d_1, d_2, \dots, d_M) \triangleq P\left(\sum_{i=1}^M \sum_{\ell=1}^{d_i} Z_{i,\ell} \leq 0\right). \quad (42)$$

The Chernoff bound on (42) is given by [6]

$$\begin{aligned} P(d_1, d_2, \dots, d_M) &< \min_{\rho > 0} E \left[e^{-\rho (\sum_{i=1}^M \sum_{\ell=1}^{d_i} Z_{i,\ell})} \right] \\ &= \min_{\rho > 0} \prod_{i=1}^M E [e^{-\rho Z_i}]^{d_i} \\ &= \prod_{i=1}^M \left\{ \prod_{j=1}^{2R} \frac{1}{1 + \bar{\gamma}_{i,j}} \right\}^{d_i} \end{aligned} \quad (43)$$

where

$$\bar{\gamma}_{i,j} \triangleq \frac{N^2 E_c}{2\sigma_{\nu(i,j)}^2} \quad (44)$$

is the average SNR of the $\nu(i, j)$ th frequency sub-band. The above result makes use of the fact that the $Z_{i,\ell}$ are independent

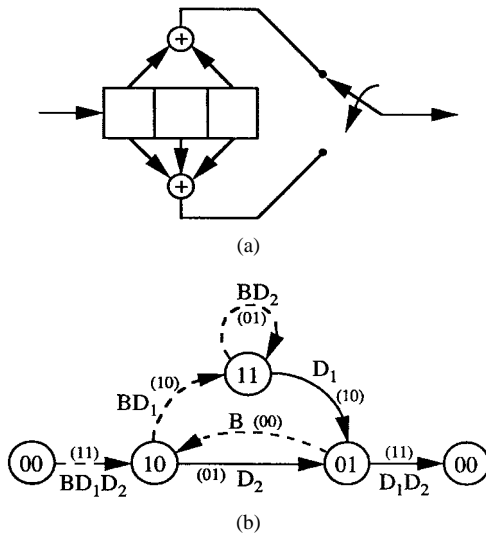


Fig. 4. Example convolutional encoder and state diagram. (a) Rate 1/2 encoder, $K = 3$. (b) Encoder state diagram.

for all i and ℓ and are identically distributed over ℓ for each fixed i .

Since the average SNR's for the transmitted symbols are assumed, in general, to be unequal, we must develop a code transfer function which enumerates not just the accumulated Hamming distance over a given error path, but the location of the errors along the path. This is best described by the example illustrated in Fig. 4. Fig. 4(a) depicts a rate 1/2 convolutional encoder of constraint length three (four states) that is frequently seen in the literature [12], [13]. This encoder would correspond to a coded multicarrier system with $M = 2$. The second figure, Fig. 4(b), is a state diagram which represents error paths of all possible lengths which exit and later remerge with the all-zeros state. Dashed lines represent transitions due to an input 1 (bit error). The output code symbols associated with each branch are shown in parentheses. Finally, each branch is labeled with monomials which indicate whether the branch corresponds to a decoder bit error (B for bit error, 1 for no bit error) and the accumulated Hamming distance, by code symbol (D_1, D_2). The code transfer function may be evaluated using signal flow techniques described in [13]. It can be shown that the transfer function for the example encoder is given by

$$T(D_1, D_2, B) = \frac{D_1^2 D_2^3 B + D_1^4 D_2^2 B^2 - D_1^2 D_2^4 B^2}{1 - 2D_2 B - D_1^2 B^2 + D_2^2 B^2}. \quad (45)$$

Note that $T(D, D, B) = D^5 B / (1 - 2DB)$, which is the result obtained in [13] wherein the location of the code symbol errors is ignored.

Thus, for an arbitrary convolutional encoder, the transfer function $T(D_1, D_2, \dots, D_M, B)$ may be used in conjunction with the Chernoff bound in (43) to union bound the probability of first-event error and the probability of bit error, respectively, as [13]

$$P_e < T(D_1, D_2, \dots, D_M, 1) \Big|_{D_i = P_i, i=1,2,\dots,M}$$

$$P_b < \frac{\partial T(D_1, D_2, \dots, D_M, B)}{\partial B} \Big|_{B=1, D_i = P_i, i=1,2,\dots,M} \quad (46)$$

where

$$P_i \triangleq \prod_{j=1}^{2R} \frac{1}{1 + \bar{\gamma}_{i,j}}, \quad i = 1, 2, \dots, M. \quad (47)$$

IV. COMPARISON TO A SINGLE-CARRIER RAKE RECEIVER

A. Assumptions

In this section, we compare a coded multicarrier system to a coded single-carrier system with a RAKE receiver having the same bandwidth. The performance of the RAKE system is derived in [6]. Here, we assume the following.

- 1) Overall system bandwidth and information rates are held equal.
- 2) The single-carrier system uses quadrature phase-shift keying chip modulation and the same convolutional code as the multicarrier system.
- 3) The average received energy over the $2MR$ multicarrier channels is equal to the average energy received over L paths in the single-carrier system.
- 4) The multipath intensity profile (MIP) is rectangular and time-invariant.
- 5) $X(f) \Leftrightarrow x(\tau)$ is a raised-cosine filter with bandwidth parameter $W = 1/(MRT_c)$ and rolloff factor β , such that $0 < \beta \leq 1$. The same filter is used in the single-carrier system, except that $W = 1/T_c$.

B. Theoretical Comparison

Since the performance of a convolutional code is ultimately governed by the average signal-to-interference-plus-noise ratios (SINR's) of the composite of code symbols, we may initially evaluate the performance of these two systems by comparing the SINR of a particular outer code symbol. Let Z_i denote the receiver test statistic corresponding to the i th symbol out of the convolutional encoder of either system ($1 \leq i \leq M$).

The SINR for the i th symbol of the multicarrier and single-carrier systems, expressed in terms of E_b and the uncoded processing gain N^u , are given, respectively, by [6]

$$\text{SINR}_i^{\text{mc}} \approx \frac{\frac{1}{M} \left(\frac{E_b}{\eta_0} \right) \left[\frac{1}{2R} \sum_{j=1}^{2R} \alpha_{1,\nu(i,j)}^2 \right]}{1 + \frac{(K_u - 1)}{N^u} \left(\frac{E_b}{\eta_0} \right) \left(1 - \frac{\beta}{4} \right)}$$

$$\text{SINR}_i^{\text{sc}} \approx \frac{\frac{1}{M} \left(\frac{E_b}{\eta_0} \right) \left[\sum_{\ell=0}^{L-1} \hat{\alpha}_{i,\ell}^2 \right]}{1 + \frac{(K_u - 1)}{N^u} \left(\frac{E_b}{\eta_0} \right) \left(1 - \frac{\beta}{4} \right)}. \quad (48)$$

The above expressions are approximate because only the dominant (i.e., first) term in the variance expansion for MAI is used in the denominator (see (26) for the multicarrier case).²

²The dominant term typically accounts for 95%–99% of the variance magnitude.

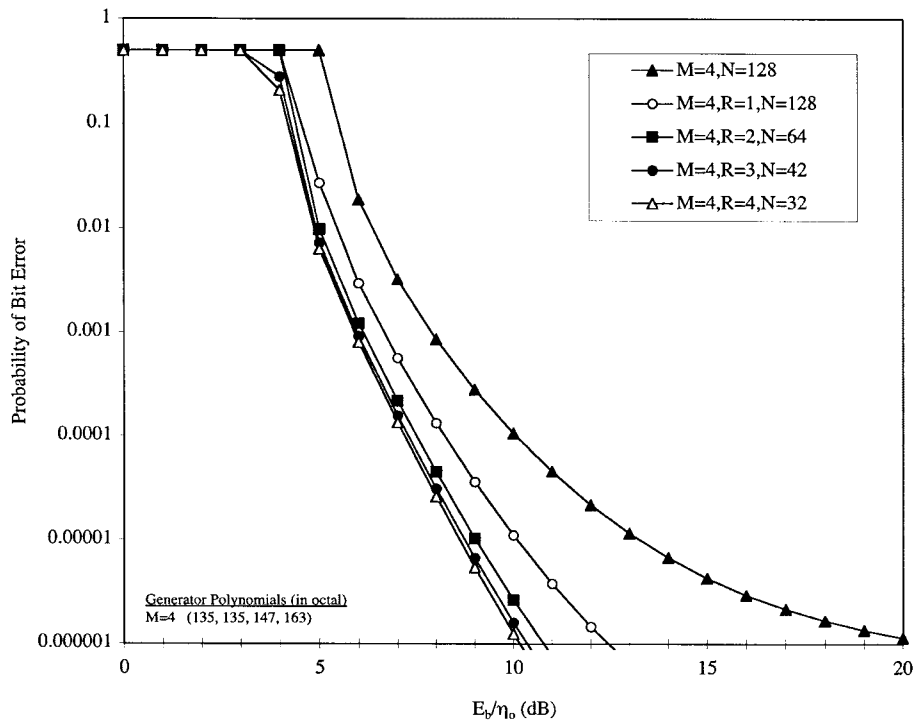


Fig. 5. BER upper bound versus E_b/η_0 varying inner-code parameter R . The outer-code parameter M is fixed at 4 (i.e., rate 1/4 code) with constraint length $K = 7$ (i.e., 64 states), and there are 100 multiple-access users. Exhibits the gain achieved by increasing the order of frequency diversity per convolutional code symbol.

In comparing these results, we note that the components in square brackets have been intentionally scaled such that they both have unit expectation.³ In fact, the SINR equations are identical *except* for the terms in square brackets, which distinguish the order of diversity experienced per code symbol in the two systems: $(2R)$ th-order frequency diversity (multicarrier) versus L th-order path diversity (single carrier). We would, therefore, expect the single-carrier system to slightly outperform the multicarrier system when $L \gg 2R$.

C. Complexity Comparison

In comparing the transmitters of the single-carrier and multicarrier systems, we immediately note that the multicarrier system is MR times as complex in terms of the number of carrier frequencies that must be synthesized. There may also be distinctions in interleaver complexity, which are outside the scope of this paper.

Of primary interest is receiver complexity. Both receivers utilize $MR = L$ in-phase and quadrature direct-sequence spread-spectrum (DSSS) demodulators. The multicarrier system uses M parallel maximal-ratio combiners ($2R$ taps each) as opposed to one serial maximal-ratio combiner in the RAKE system (L taps). The remainder of the receivers of the two systems are virtually identical, most notably the soft-decision Viterbi decoder. Since both systems employ the same Viterbi decoder and employ the same number of DSSS demodulators, we argue a *similar* receiver complexity in the two systems considered.

³This is justified by the assumption of equal received energy per bit.

V. NUMERICAL RESULTS

A. Multicarrier System Parameters

Given a fixed information rate and total bandwidth allocation, the product MRN must be held constant, where N is the processing gain per subcarrier. Increasing the parameter M will yield lower rate (i.e., stronger) codes, allowing the system to better combat MAI and fading. On the other hand, increasing the parameter R will primarily improve the extent to which the system can combat multipath fading, through diversity. Lastly, increasing N will improve the mitigation of MAI. Clearly, the improvement in performance due to increasing any one parameter is offset by degradation in performance as a result of decreasing the other parameter(s). This three-way tradeoff suggests the existence of an optimal set of parameters for a given scenario and desired performance.

Suppose we fix the single-carrier system's uncoded processing gain N^u at some specified value. Then, the parameters M, R and N must satisfy $N^u = MRN$. We opt to specify parameters M and R and leave the parameter N to be defined as $N = \lfloor N^u/MR \rfloor$.

In this section, we assume the use of a raised-cosine filter characteristic, with rolloff factor $\beta = 0.5$, for pulse shaping. We further assume the uncoded processing gain to be fixed at $N^u = 512$. We assume the use of maximal-length pseudonoise (PN) spreading sequences with periods exceeding the subcarrier processing gain N . All convolutional encoders considered in this paper are based on maximal free distance codes defined in [14].

For fixed M , varying the parameter R will specify the order of frequency diversity per convolutionally coded symbol. In

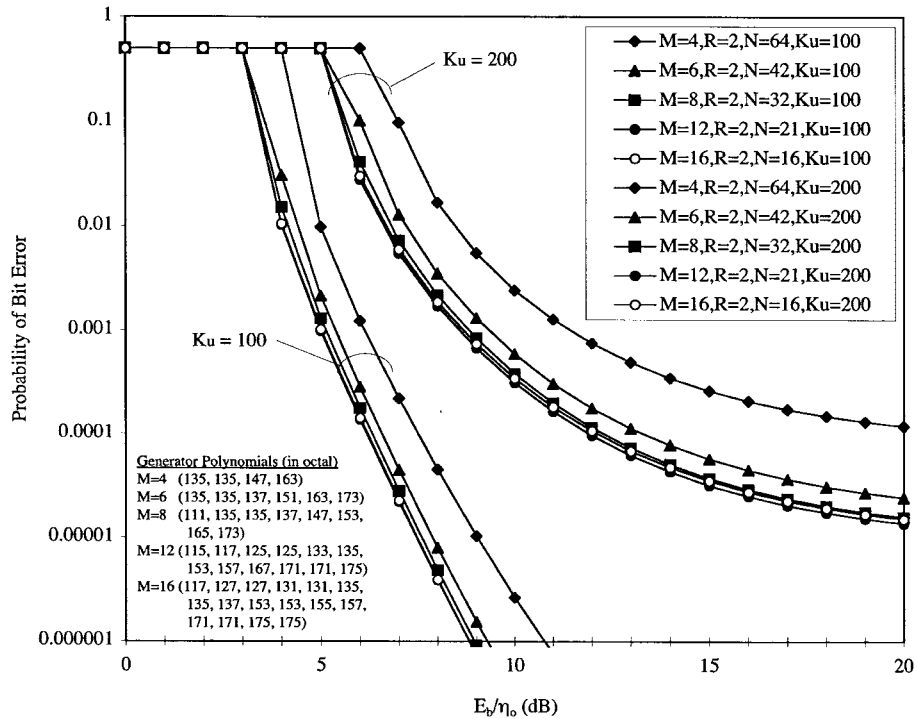


Fig. 6. BER upper bound versus E_b/η_0 varying outer-code parameter M with fixed constraint length $K = 7$. The inner-code parameter R is fixed at 2 and there are either 100 or 200 multiple-access users. It illustrates the gain achieved by increasing M and the corresponding degradation due to decreasing the processing gain N .

Fig. 5, we plot the upper bound on the probability of bit error obtained in (46) versus E_b/η_0 and allow R to vary from 1 to 4, with M and K fixed. Specifically, we fix the number of users at 100 and use a rate $1/4$ code of constraint length $K = 7$ (i.e., 64 states), corresponding to the case $M = 4$. The rightmost curve depicts the performance of the system proposed in [4] and [5], where each coded symbol is transmitted over one flat-fading frequency diversity branch. In the $R = 1$ case, second-order frequency diversity is obtained due to the in-phase and quadrature mapping of each coded symbol. For $R = 2$, the system experiences fourth-order frequency diversity per coded symbol. For values of R greater than two, there is a negligible improvement.⁴ This result is consistent with historical observations on the performance of ideal coherent maximal-ratio combiner systems [17]; namely, that there are marginally decreasing gains for diversity orders beyond three or four. We therefore take R to be fixed and equal to two throughout the remainder of this paper. It is worth mentioning, however, that larger values of R might be desirable from a standpoint of combating NBI insofar as the smaller multicarrier sub-bands will tend to better isolate the interference, allowing the maximal-ratio combiner to more effectively attenuate the affected signals. Suppression of NBI is the topic of Part II of this paper.

Next, we consider the parameter M and the explicit tradeoff between M and N . In Fig. 6, we plot the upper bound on the probability of bit error versus E_b/η_0 and allow M to take on values 4, 6, 8, 12, and 16. We fix the number of users at either

⁴For other values of M and K , one sees similar marginal improvements when increasing R .

100 or 200 and use rate $1/M$ codes of constraint length 7, with $R = 2$. For $K_u = 100$, we see that increasing M yields improved performance, but with marginal successive gains, due to the fact that decreases in code rate are accompanied by increases in the power of MAI (due to smaller N). In fact, for $K_u = 200$, the $M = 12$ system outperforms the $M = 16$ system. Thus, for a target user capacity, a reasonable choice for M is suggested such the performance is close to optimal, and M is minimized so as to minimize receiver complexity. For 100 users, it would appear that either $M = 6$ or $M = 8$ represents a good choice.

B. System Comparison with AWGN and MAI

In Fig. 7, we plot the upper bound on the bit-error rate (BER) for single-carrier and multicarrier systems as a function of the energy-per-bit-to-noise spectral density E_b/η_0 , with the number of multiple-access users K_u , equal to both 100 and 200, using a rate $1/6$, constraint length 9 (256 state) code. At 200 users and a BER of 10^{-3} , the 0.5-dB difference represents the performance gain due to twelfth-order path diversity of the RAKE system versus the fourth-order frequency diversity in the multicarrier system. This gain is diminished as K_u decreases. We see a similar result when plotting the upper bound on BER as a function of K_u , as shown in Fig. 8, for an $M = 8$ multicarrier system. The single-carrier system is capable of supporting slightly more users at a given BER and E_b/η_0 . Therefore, the general conclusion is that the two systems are nearly identical in performance at very similar complexity. Part II of this paper will continue the system comparison in the presence of various forms of NBI.

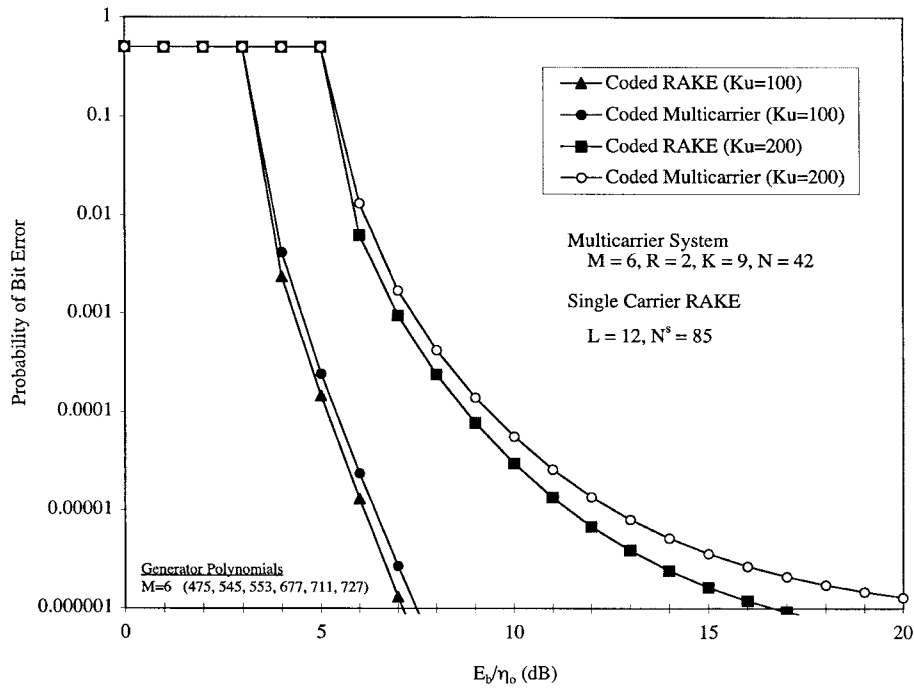


Fig. 7. BER upper bound versus E_b/η_0 (dB), for $K_u = 100$ and 200 . It indicates the gain in decibels of coded single-carrier DS-CDMA system over an identically coded multicarrier DS-CDMA system in the presence of AWGN and MAI and assumes a rectangular MIP.

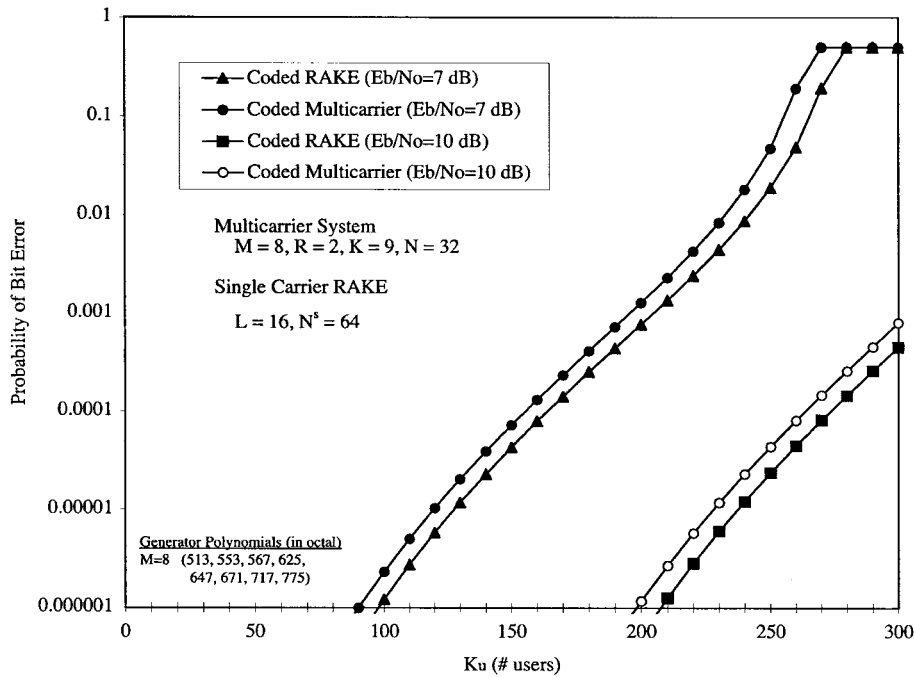


Fig. 8. BER upper bound versus K_u , for $E_b/\eta_0 = 7$ dB and 10 dB. It demonstrates the gain in user capacity of a coded single-carrier DS-CDMA system over an identically coded multicarrier DS-CDMA system in the presence of AWGN and MAI and assumes a rectangular MIP.

C. Exponential Multipath Intensity Profile

The results in the preceding section are predicated on the assumption of a flat, or rectangular, MIP. In this section, we relax the assumption of a rectangular MIP to assess the effects of a variable MIP on the system comparison. Since the multicarrier chip duration exceeds the delay spread of the channel, all of the multipath energy is collected in one effective resolvable path and, therefore, is not dependent on

the shape of the MIP. However, for the single-carrier system, the RAKE receiver combines received signals from several resolvable path delays, and thus, the structure of the MIP will affect the resulting performance.

We consider the L -path fade amplitudes for the single-carrier channel. For a rectangular MIP, we have $E[\hat{\alpha}_\ell^2] = 1/L$, whereas, in general, the $E[\hat{\alpha}_\ell^2] \triangleq \Gamma_\ell$ need not be equal for different values of ℓ . For the exponential MIP [12] and L

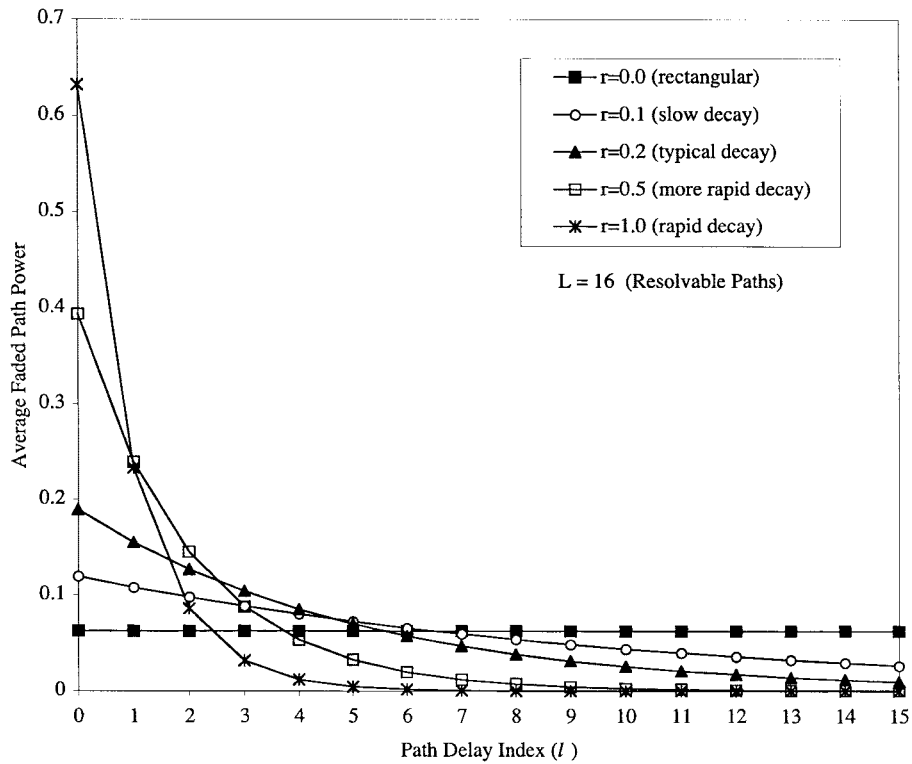


Fig. 9. MIP's for $L = 16$. It indicates average path power at successive chip delays from the first received path. Specifically, we plot $E[\hat{\alpha}_\ell^2] \triangleq \Gamma_\ell = Ce^{-r\ell}$ for various values of r (C is a normalization constant).

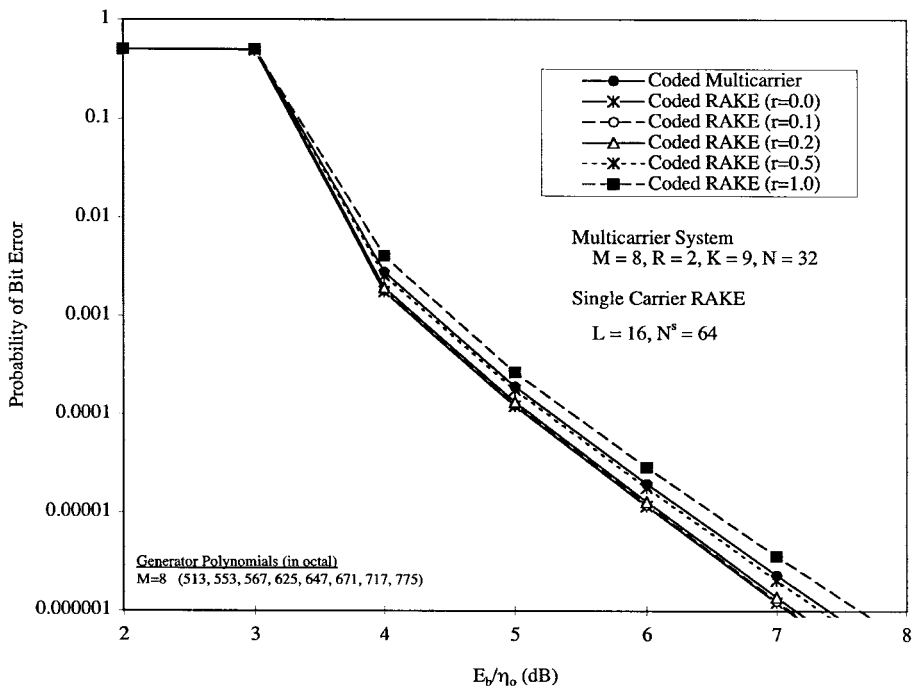


Fig. 10. BER upper bound versus E_b/η_0 (dB), exponential MIP. It examines the effect of an exponential MIP on the performance of a coded single-carrier DS-CDMA system and shows that when relaxing the rectangular MIP assumption, the single-carrier system performance can, in fact, become worse than that of the multicarrier system, for sufficiently large exponential decays.

resolvable paths, we define $\Gamma_\ell \triangleq Ce^{-r\ell}$, where r is a decay factor and C is a normalizing constant. Fig. 9 depicts the MIP's corresponding to several decay factors of interest, where we assume $L = 16$ resolvable paths.

For each MIP shown in Fig. 9, we compare the performance of an $M = 8, R = 2$ multicarrier system to that of a single-carrier system with $L = 16$ resolvable paths. In Fig. 10, one notes that as the decay factor r is increased, the single-carrier

performance tends toward that of the multicarrier system. For the rapid decay rate of 0.5, the two systems exhibit nearly identical performance, and for the very rapid decay of 1.0, the multicarrier system outperforms the single-carrier system by several tenths of a decibel.

The general conclusion is that the rectangular MIP assumption is most beneficial to the single-carrier system, and when we consider a more realistic exponential MIP, the single-carrier performance becomes worse, rendering the performance of the two systems closer.

VI. CONCLUSION

In this paper, we discussed a new way of realizing a wide-band CDMA system that embodies robustness to multipath fading and mitigation of MAI. The proposed system was shown to provide coded performance which is comparable to that of a classical single-carrier DS-SS system at similar receiver complexity. The multicarrier system employs band-limited narrow-band DS-SS waveforms which can be positioned in a flexible manner; this may be an advantage over the conventional DS-SS system in situations where only a noncontiguous spectrum is available. Part II of this paper will analyze the capability of the proposed system to suppress NBI, without the need for a front-end interference suppression or a notch filter (i.e., at no additional complexity).

REFERENCES

- [1] G. L. Turin, "Introduction to spread-spectrum antimultipath techniques and their application to urban digital radio," *Proc. IEEE*, vol. 68, pp. 328–353, Mar. 1980.
- [2] M. K. Simon, J. K. Omura, R. A. Scholtz, and B. K. Levitt, *Spread Spectrum Communications Handbook*. New York: McGraw-Hill, 1994.
- [3] S. Kondo and L. B. Milstein, "On the performance of multicarrier DS-SS systems," *IEEE Trans. Commun.*, vol. 44, pp. 238–246, Feb. 1996.
- [4] D. N. Rowitch and L. B. Milstein, "Coded multicarrier code division multiple access," in *Proc. 1995 Int. Symp. Information Theory*, Whistler, BC, Canada, Sept. 1995, p. 23.
- [5] ———, "Convolutional coding for direct sequence multicarrier CDMA," in *Proc. MILCOM'95*, San Diego, CA, Nov. 1995, pp. 55–59.
- [6] D. N. Rowitch, "Convolutional and turbo coded multicarrier direct sequence CDMA, and applications of turbo codes to hybrid ARQ communication systems," Ph.D. dissertation, Univ. of California at San Diego, June 1998.

- [7] H. Sari, G. Karam, and I. Jeanclaude, "An analysis of orthogonal frequency division multiplexing for mobile radio applications," in *Proc. VTC'94*, Stockholm, Sweden, June 1994, pp. 1635–1639.
- [8] L. B. Milstein, D. L. Schilling, R. L. Pickholtz, V. Erceg, M. Kullback, E. G. Kanterakis, D. S. Fishman, W. H. Biederman, and D. C. Salerno, "On the feasibility of a CDMA overlay for personal communications networks," *IEEE J. Select. Areas Commun.*, vol. 10, pp. 655–667, May 1992.
- [9] T. Eng and L. B. Milstein, "Comparison of hybrid FDMA/CDMA systems in frequency selective Rayleigh fading," *IEEE J. Select. Areas Commun.*, vol. 12, pp. 938–951, June 1994.
- [10] D. N. Rowitch and L. B. Milstein, "Coded multicarrier DS-SS in the presence of partial band interference," in *Proc. MILCOM'96*, McLean, VA, Nov. 1996, pp. 204–209.
- [11] J. Bingham, "Multicarrier modulation for data transmission: An idea whose time has come," *IEEE Commun. Mag.*, vol. 28, pp. 5–14, May 1990.
- [12] J. Proakis, *Digital Communications*. New York: McGraw-Hill, 1989.
- [13] A. J. Viterbi, "Convolutional codes and their performance in communication systems," *IEEE Trans. Commun.*, vol. COM-19, pp. 751–772, Oct. 1971.
- [14] R. Palazzo Jr., "A network flow approach to convolutional codes," *IEEE Trans. Commun.*, vol. 43, pp. 1429–1440, Apr. 1995.
- [15] W. Xu and L. B. Milstein, "On the performance of multicarrier RAKE systems," *IEEE Trans. Commun.*, submitted for publication.
- [16] R. E. Ziemer and N. Nadgouda, "Effect of correlation between sub-carriers of an MCM/DSSS communication system," in *Proc. VTC'96*, Atlanta, GA, Apr. 1996, pp. 146–150.
- [17] S. Stein, "Fading channel issues in system engineering," *IEEE J. Select. Areas Commun.*, vol. SAC-5, pp. 68–89, Feb. 1987.



Douglas N. Rowitch (S'94–M'98) received the B.A. degree in applied mathematics in 1984, the M.A. degree in applied mathematics in 1984, the M.S.E.E. degree in 1994, and the Ph.D. degree in 1998 from the University of California at San Diego.

He joined Qualcomm Incorporated, San Diego, CA, in 1998, where he is a Staff Engineer working on third-generation wireless standards and associated ASIC developments, with primary emphasis on turbo-codes. His research interests include coding theory, spread spectrum, and communication theory.

Laurence B. Milstein (S'66–M'68–SM'77–F'85), for a photograph and biography, see p. 88 of the January 1999 issue of this TRANSACTIONS.